



## OPEN ACCESS

## EDITED BY

Jingjun Wu,  
Zhejiang University, China

## REVIEWED BY

Xiaozhen Zhang,  
Jingdezhen Ceramic Institute, China  
Guoxiong Wang,  
Dalian Institute of Chemical Physics  
(CAS), China

## \*CORRESPONDENCE

Xiangang Luo,  
✉ lxg@ioe.ac.cn  
Kui Xie,  
✉ kxie@fjirsm.ac.cn

## SPECIALTY SECTION

This article was submitted to Polymeric  
and Composite Materials,  
a section of the journal  
Frontiers in Materials

RECEIVED 01 March 2023

ACCEPTED 22 March 2023

PUBLISHED 06 April 2023

## CITATION

Liu K, Cheng F, Luo Y, Liu L, Wang C, Xie K  
and Luo X (2023), Porous single  
crystalline-like titanium dioxide monolith  
with enhanced  
photoelectrochemical performance.  
*Front. Mater.* 10:1177093.  
doi: 10.3389/fmats.2023.1177093

## COPYRIGHT

© 2023 Liu, Cheng, Luo, Liu, Wang, Xie  
and Luo. This is an open-access article  
distributed under the terms of the  
[Creative Commons Attribution License  
\(CC BY\)](https://creativecommons.org/licenses/by/4.0/). The use, distribution or  
reproduction in other forums is  
permitted, provided the original author(s)  
and the copyright owner(s) are credited  
and that the original publication in this  
journal is cited, in accordance with  
accepted academic practice. No use,  
distribution or reproduction is permitted  
which does not comply with these terms.

# Porous single crystalline-like titanium dioxide monolith with enhanced photoelectrochemical performance

Kaipeng Liu<sup>1,2,3</sup>, Fangyuan Cheng<sup>3</sup>, Yunfei Luo<sup>1,3</sup>, Ling Liu<sup>1,3</sup>,  
Changtao Wang<sup>1,3</sup>, Kui Xie<sup>4\*</sup> and Xiangang Luo<sup>1,3\*</sup>

<sup>1</sup>State Key Laboratory of Optical Technologies on Nano-Fabrication and Micro-Engineering, Institute of Optics and Electronics, Chinese Academy of Sciences, Chengdu, China, <sup>2</sup>School of Optoelectronic Science and Engineering, University of Electronic Science and Technology of China, Chengdu, China, <sup>3</sup>School of Optoelectronics, University of Chinese Academy of Sciences, Beijing, China, <sup>4</sup>Key Laboratory of Design and Assembly of Functional Nanostructures, Fujian Institute of Research on the Structure of Matter, Chinese Academy of Sciences, Fuzhou, China

Macro-sized porous single crystalline-like (PSC-like) TiO<sub>2</sub> is endowed with unique structural advantages due to its structural consistency and porosity in a large area, which would significantly enhance its photoelectrochemical function. However, there are significant technical challenges in the growth of porous single crystalline-like monoliths. The consistency of structure dominates the structure so that the grain boundary is reduced to the minimum, which is in contradiction with the three-dimensional percolation structure. Here we report a lattice reconstruction strategy based on solid-solid transformation to grow porous single crystal-like anatase TiO<sub>2</sub> dominated by (200) and (101) facets at 2 cm scale. In comparison with the traditional definition of porous single crystal, it has two different lattice orientations, but still has good photoelectrochemical properties. The band gap engineering introduces Ti<sup>3+</sup> gap into the lattice to generate Ti<sub>n</sub>O<sub>2n-1</sub> with Magneli phase, limiting the created active structure to the lattice with two-dimensional surface, which would open a new avenue to create highly active surfaces to capture photons and transport electrons stably. The PSC-like Ti<sub>n</sub>O<sub>2n-1</sub> provides enhanced exciton lifetime (3–5 ns) as a photocatalytic catalyst and shows significant visible light absorption. The independent PSC-like Ti<sub>n</sub>O<sub>2n-1</sub> delivers high photocurrent of 1.8–5.5 mA · cm<sup>-2</sup> at room temperature and does not decay for 10 h.

## KEYWORDS

porous crystal, titanium dioxide, magneli phase, photoelectricity, catalysis

## 1 Introduction

The surface of transition metal oxides is usually used to carry the reaction of electron transfer and proton coupling, which is very important for the solar energy conversion process (Schrauben et al., 2012; Guo et al., 2019). Among photocatalysts, Ti-based semiconductor materials provide the high photocatalytic activity and play a key role in photocatalysis and solar energy conversion (Zhao et al., 2019; Chen et al., 2020). As an n-type photoanode, the band gap of titanium dioxide is about 3.2eV, and its energy conversion efficiency is often limited by the effective absorption of visible light and the rapid recombination of electrons and holes. In the process of modification of traditional

nano-photocatalytic materials, nitrogen doping with unsaturated coordination structure is widely used to change the catalytic properties of materials (Bie et al., 2019; Meng et al., 2019; Xu et al., 2020). However, the metal-nitrogen group with immeasurable nitrogen coordination has structural disturbance in its catalytic activity, which is frequently accompanied by poor stability and dependability.

Anatase titanium dioxide is one of the transition metal oxide photocatalysts discussed in recent years because of its high photocatalytic activity due to its structural characteristics. As a typical traditional photocatalyst, its conduction band composed of valence electrons and empty orbitals is well understood. The  $\text{Ti}^{4+}$  and bridging  $\text{O}^{2-}$  ions are staggered along the [101] axis, providing convenience for electronic structure adjustment (Li et al., 2006; Guo et al., 2016). Generally, titanium dioxide semiconductor with a broadband gap of  $\sim 3.2\text{eV}$  is exposed to sunlight as the light collection device, and its absorption of visible light is limited, and the collection rate of light source at near-infrared wavelength is extremely low. Affected by its electronic structure, the conduction band of  $\text{TiO}_2$  receives the electrons excited from the valence band, and forms a high-energy and easily mobile electron-hole pair with the valence band structure with holes. Electron-hole pairs are usually used as medium to participate in the chemical reaction on the catalyst surface and reassemble to release heat and light energy. In addition, the electron-hole pair would also be dissociated again and transferred to the active site of the catalyst in the form of free electrons to form surface groups (Kou et al., 2017; Chen and Ardo, 2018). In this process, the band gap adjustment strategy and the sufficient reaction sites provided by the high specific surface are the keys to determine the photocatalytic performance (Li et al., 2022).

Different from the strategy of doping impurities into titanium dioxide lattice to form point defects, the  $\text{Ti}_n\text{O}_{2n-1}$  with Magneli phase effectively enhances the absorption of visible light through the self-doping of  $\text{Ti}^{3+}$ . The doping strategy with point defects is to achieve effective absorption of visible light by reducing the conduction band or increasing the valence band (Yu et al., 2013; Faraji et al., 2019). However, traditional black titanium dioxide prepared by hydrogenation often forms core-shell nanoparticles covered by  $\text{Ti}^{3+}$  disordered phase on the surface. The crystal structure that cannot be accurately confirmed and too many grain boundaries will greatly hinder the rapid transport of electrons. Here we adjust the electronic structure of the material to achieve enhanced absorption of visible and infrared light by introducing  $\text{Ti}^{3+}$  gap into PSC-like  $\text{Ti}_n\text{O}_{2n-1}$  crystal to produce local defect structure (Cheng et al., 2019).

Titanium dioxide is usually used as the photoanode in the photochemical cell, and the direct catalytic splitting of water under light irradiation and external bias is one of the most active topics (Qian et al., 2019; Zhang et al., 2019; Bie et al., 2022). Generally, photogenic holes on the surface of titanium dioxide photoanode would activate water in the electrolyte to generate surface OH, while the electrons are transferred to the opposite electrode to reduce protons to hydrogen (Liu et al., 2019; Ros et al., 2020). The generation of OH is the key to the realization of photocatalytic water, which would provide opportunities for the participation of highly active hydroxyl radicals in heterogeneous catalysis, and shows great potential in basic and applied research (Shin et al., 2022).

In this work, the lattice reconstruction strategy based on the phase transformation is used to fabricate the PSC-like  $\text{Ti}_n\text{O}_{2n-1}$  monoliths at 2 cm scale (Jin et al., 2020; Xiao and Xie, 2022). PSC-like  $\text{Ti}_n\text{O}_{2n-1}$  monoliths has a high monocrystal-like property, and its dominant lattice structure maintains a high consistency with bulk single crystal. Its surface well-defined structure with clear and long-range order at atomic scale significantly reduces the scattering effect of electrons/holes caused by the interface between traditional grains, which will significantly enhance the functionality of charge separation and transmission required to inhibit charge recombination. Moreover, the PSC-like  $\text{Ti}_n\text{O}_{2n-1}$  monoliths possess a large specific surface area, which makes them suitable as photoanodes in photoelectrochemical cells. This provides ample reaction sites for photocatalytic reactions and facilitates the collection of electrons/holes, resulting in ultra-high photocurrent and water decomposition performance.

## 2 Materials and methods

### 2.1 Crystal growth

The growth of precursor  $\text{KTiOPO}_4$  (KTP) single crystal is achieved by the topseed crystal method with molybdate as the cosolvent (Jacco et al., 1984). KTP single crystal with (110) faces is directionally cut and polished to  $10\text{ mm} \times 10\text{ mm} \times 0.5\text{ mm}$  for growth of PSC-like anatase  $\text{TiO}_2$ . The KTP single crystal is introduced into the vacuum tube furnace that can accurately control the pressure and temperature, and  $100\text{--}200\text{ sccm H}_2/\text{Ar}$  gas flow is introduced to control the pressure to stabilize to  $67\text{--}333\text{ mbar}$ . KTP is maintained at  $600^\circ\text{C}\text{--}950^\circ\text{C}$  for  $10\text{--}30\text{ h}$  in a strong reducing atmosphere to generate PSC-like anatase  $\text{Ti}_n\text{O}_{2n-1}$  monoliths of Magneli phase.

### 2.2 Characterizations

We detect the formation of the phase and determined the orientation of the crystal plane on the X-ray diffractometer (XRD, Mniflex 600). Then the porous morphology of the crystal material is observed by field emission scanning electron microscopy (FE-SEM, SU8010). TEM samples are prepared by using FIB (Zeiss Auriga), selected area electron diffraction (SAED) tests are carried out at  $200\text{ kV}$  accelerating voltage. The crystal structure is characterized on spherical aberration corrected high resolution transmission electron microscope (Cs-HRTEM) (FEITitan3G2 60–300) at  $300\text{ kV}$  accelerating voltage. X-ray photoelectron spectroscopy (XPS, Escalab 250Xi) determines the chemical state of Ti in  $\text{Ti}_n\text{O}_{2n-1}$ . The electron paramagnetic resonance (EPR) spectrums are obtained on JES TE200 (JEOL) to evaluate the signals of  $\text{Ti}^{3+}$  and oxygen vacancies. The performance test of photoelectric decomposition water is carried out in  $1\text{M NaOH}$  solution at  $25^\circ\text{C}$ .

### 2.3 Photoelectrochemical measurement

In the photoelectrochemical test, we use the three-electrode test method. The electrochemical workstation (IM6, Zahner) is

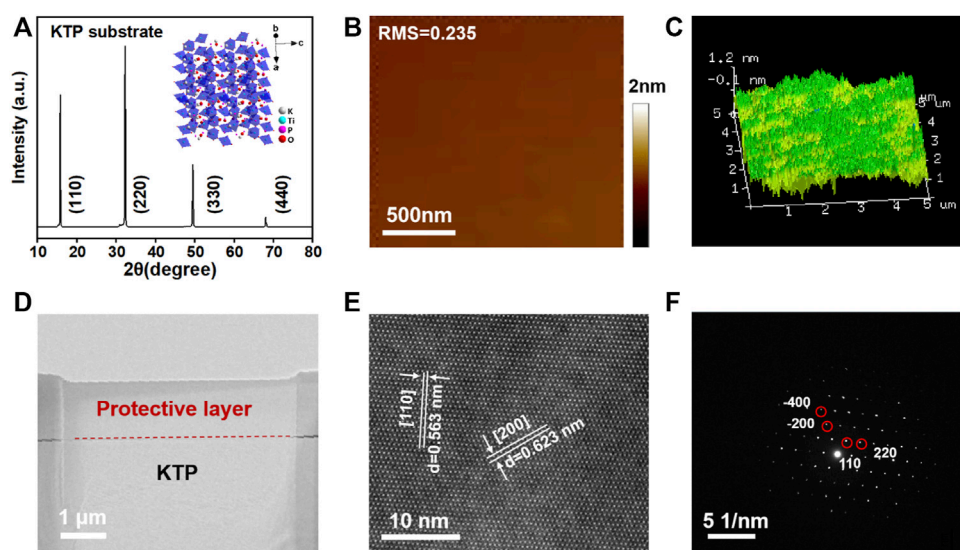


**FIGURE 1**

(A) XRD pattern of (110) KTP single crystal, the inset is crystal structure of KTP and lattice channel of K/P removal along (110) facet. (B) Surface roughness. (C) Surface 3D AFM image of KTP substrate. (D) TEM image of KTP slice. (E) Spherical aberration corrected Scanning Transmission Electron Microscope (Cs-HRTEM) image of the KTP view towards [110] plane. (F) SAED pattern of KTP.

equipped with a two-chamber photocatalyst cell with Pt and saturated calomel electrode as the counter electrode and reference electrode, respectively. In addition, PSC-like  $\text{Ti}_n\text{O}_{2n-1}$  monoliths are used as the working electrode, which is separated by an anion exchange membrane (Nafion 212). The photoelectric decomposition of water is tested in 1M sodium hydroxide solution at 25°C. The Nernst equation is that to convert all potentials to RHE reference scale:

$$E_{\text{RHE}} = E_{\text{Hg}/\text{Hg}_2\text{Cl}_2} + 0.0591 \times \text{pH} + 0.244$$

### 3 Results and discussion

The growth of porous single crystalline-like  $\text{TiO}_2$  is a dynamic equilibrium process between heat and force. We grow and treat (110) KTP (10 mm × 10 mm × 0.5 mm) to grow PSC-like anatase  $\text{TiO}_2$  monoliths with the identical dimension in a reducing atmosphere at 600–950°C and 67–333 mbar. It is well known that titanium dioxide is a typical photoelectric semiconductor with different crystal configurations such as rutile and anatase. The growth process of PSC-like rutile  $\text{TiO}_2$  often requires higher operating temperatures to drive the phase transition, which remains technically difficult. There is a strong dependence between the formation of PCS-like  $\text{Ti}_n\text{O}_{2n-1}$  crystal rate and the crystal quality of KTP precursor. In the process of solid-solid phase transformation, the growth process of recrystallization is more sensitive to the surface roughness of the parent crystal. In Figure 1A, the sharp characteristic peak in the XRD pattern indicates that KTP with (110) facets has high single crystal quality. In inset image, the K and P atom escape channels along the KTP (110) facet are not completely unobstructed, which is one of

the reasons for the appearance of competitive crystal planes in addition to the dominant crystal planes during the PSC-like  $\text{TiO}_2$  monolith growth process. As shown in Supplementary Figure S1, the Raman spectroscopy and SEM picture indicate the smooth uniform structure in KTP. We polish the KTP substrate to maintain its surface roughness below 0.24 nm as shown in Figure 1B; Figure 1C shows the flatness of KTP at the three-dimensional nanometer scale under the atomic force microscope. We used focused ion beam (FIB) to prepare the sample of Transmission Electron Microscope (TEM), that is (110) KTP slice with ~50 nm thickness as shown in Figure 1D, which coupled with Cs-HRTEM to observe the lattice structure of mother crystal KTP in the field, as shown in Figure 1E. The uniform distribution of K, Ti, P, and O elements in the form of regular periodic arrays re-certified the surface well-defined structure of the single crystal to accommodate the order of solid-solid phase transformation to Ti-O coordination structure. The lattice spacing of 0.563 nm and 0.623 nm are certified as [110] and [200] facets of KTP, respectively, which is consistent with the structure of the selected area electron diffraction pattern (SAED), as shown in Figure 1F (Sorokina and Voronkova, 2007). Breaking the KTP single crystal structure as the starting step of the lattice reconstruction process, the long range ordered crystal structure of the single crystal is the key to the formation of the porous single crystalline  $\text{TiO}_2$  nucleus. In order to accelerate the growth of porous single crystalline-like monolith, the mother phase should be single crystalline state to enable stable solid-solid transformation (Li and Xie, 2023).

Porous single crystal monoliths have the unique advantage in the construction of well-defined structures at surface interfaces by combining the consistency of the structure with the porous structure. Porous single crystalline-like monoliths retain a porous skeleton and the grain boundary region is minimized to ensure a high single crystal rate. In Supplementary Figure S2, The PSC-like

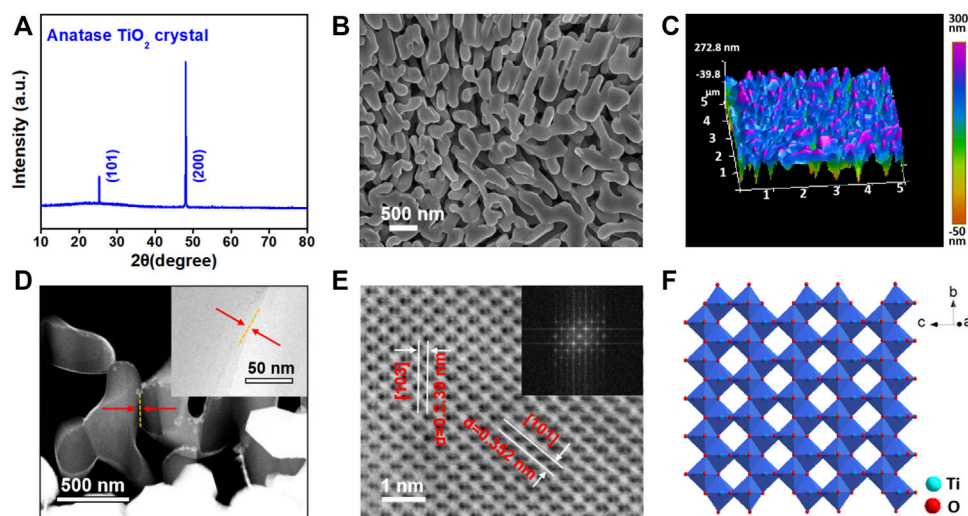


FIGURE 2

(A) XRD pattern of PSC-like anatase  $\text{TiO}_2$ . (B) The SEM image of PSC-like anatase  $\text{TiO}_2$  monolith. (C) Surface 3D AFM image of  $\text{TiO}_2$  with porous structure. (D) STEM image of the PSC-like  $\text{TiO}_2$ , the inset image is TEM at the corresponding interface. (E) Cs-HRTEM image of PSC-like  $\text{Ti}_{38}\text{O}_{75}$  viewed towards  $[-1-31]$  axis. (F) The illustration is the structure of anatase  $\text{TiO}_2$ .

anatase  $\text{TiO}_2$  is grown on the solid-solid phase transformation, and adjusted the single crystal rate by adjusting the annealing process to reduce the longitudinal temperature gradient. The higher the annealing rate, the faster the transverse and longitudinal surface stress changes, which means a lower single crystal rate. Figure 2A shows the XRD pattern of PSC-like anatase  $\text{TiO}_2$  dominated by (200) facet. The characteristic peaks of low exponent observed at  $25.28^\circ$  are consistent with the orientation [101] of anatase  $\text{TiO}_2$ , indicating competitive growth between crystal facets, which is due to a high lattice mismatch of  $\sim 23.58\%$  between (110) KTP and (200)  $\text{TiO}_2$  (Jiang et al., 2011). Figure 2B and Figure 2C show the microstructure of PSC- $\text{TiO}_2$  growing along the (110) KTP, which with pore size of  $\sim 150$  nm. The crystal scale of PSC-like  $\text{TiO}_2$  remains unchanged relative to KTP, while the directional removal of K/P as the target atom results in the reduction of the overall atomic density to form pores. We further confirmed the  $\text{TiO}_2$  transformation using EDS and elemental mapping, as shown in Supplementary Figure S3. Figure 2D shows the STEM image of PSC  $\text{TiO}_2$  monolith, confirming the 3D interconnected channel structure at  $\sim 100$ – $200$  nm. It is noteworthy that the annealing process is one of the methods to adjust the dislocation density in PSC-like  $\text{TiO}_2$  monolith. The very small areas in PSC-like  $\text{TiO}_2$  monolith evolves from sub-grain boundary to grain boundary during the recrystallization process. Figure 2E shows the Cs-HRTEM image of the skeleton in PSC-like  $\text{TiO}_2$  framework. The introduction of a small amount  $\text{Ti}^{3+}$  causes the random dislocations in PSC  $\text{Ti}_{38}\text{O}_{75}$  monolith, while a periodic dislocation such as  $\text{Ti}_9\text{O}_{17}$  is shown in Supplementary Figure S4 with a large number of  $\text{Ti}^{3+}$  gaps. The chemical formula of  $\text{Ti}_n\text{O}_{2n-1}$  is determined by the oxidation of graphite in a vacuum system. The SAED image of Fourier transform shown in the Figure 2F confirms that it is also a typical tetragonal single-crystalline structure.

The peaks of Raman spectroscopy at 145, 197, 395, and  $515\text{ cm}^{-1}$  are observed in Figure 3A, although slight Raman shift is observed, they are still consistent with the crystal structure of anatase phase

(Es-Souni et al., 2008). We use X-ray photoelectron spectroscopy (XPS) to study the evolution of the Ti chemical state in the surface of PSC-like  $\text{TiO}_2$  under an Ar atmosphere. The surface Ti is mainly +4 in  $\text{Ti}_{38}\text{O}_{75}$  as shown in Figure 3B, indicating that there is sufficient oxidation state in the lattice. The EPR spectrum in Figure 3C confirms the coexistence of  $\text{Ti}^{3+}$  and a small amount of oxygen vacancy on the surface of PSC  $\text{Ti}_{38}\text{O}_{75}$  monolith, the signal index increases when the n value are reduced to 9. The loss of oxygen means that the n value decreases in  $\text{Ti}_n\text{O}_{2n-1}$ , resulting in more  $\text{Ti}^{4+}$  being reduced to  $\text{Ti}^{3+}$  gap. Which would adjust the electronic and band gap structure of  $\text{TiO}_2$  to expand the visible-infrared light absorption, as shown in Figure 3D. The presence of the high concentration of  $\text{Ti}^{3+}$  interstitials in PSC-like  $\text{Ti}_9\text{O}_{17}$  monolith with the magneli phase actually transforms it into a black electronic conductor. The transient absorption spectrum of PSC-like  $\text{Ti}_n\text{O}_{2n-1}$  (n = 9 and 38) are further studied under the excitation wavelength of 523 nm. As shown in Figure 3E and Figure 3F, the ultra-long exciton lifetime ( $\sim 4.7$  ns) in PSC-like  $\text{Ti}_n\text{O}_{2n-1}$  (n = 9 and 38) monoliths is verified, which the lifetime is  $\sim 5$  times that of polycrystalline materials. This result indicates that the inhibition of structural coherence on charge recombination is significantly enhanced.

The precise adjustment of the electronic structure of  $\text{TiO}_2$  can achieve the maximum photocurrent response of light collection and increase the specific surface area of porous structure to enhance the photocatalytic performance. Here we use a three-electrode setup to study the photocurrent performance of PSC-like  $\text{TiO}_2$ , as Figure 4A shown. In Figure 4B, we further used Linear Scanning Voltammetry to test the photocurrent-potential curve of PSC-like  $\text{Ti}_n\text{O}_{2n-1}$  (n = 9 and 38) photoelectrode in 1M NaOH electrolyte solution. Under 10 times air mass (AM) 1.5G illumination of simulated sunlight, the photocurrent generated by PSC-like  $\text{Ti}_9\text{O}_{17}$  photoanode could be as high as  $5.5\text{ mA} \cdot \text{cm}^{-2}$  at an external bias voltage of 1.6V. In addition, the initial potential of the PSC-like  $\text{Ti}_9\text{O}_{17}$  electrode for water decomposition is  $\sim 0.1$  V in a 0.5M  $\text{Na}_2\text{SO}_4$  electrolyte solution under illumination intensity of 10 AM 1.5 G. In Supplementary

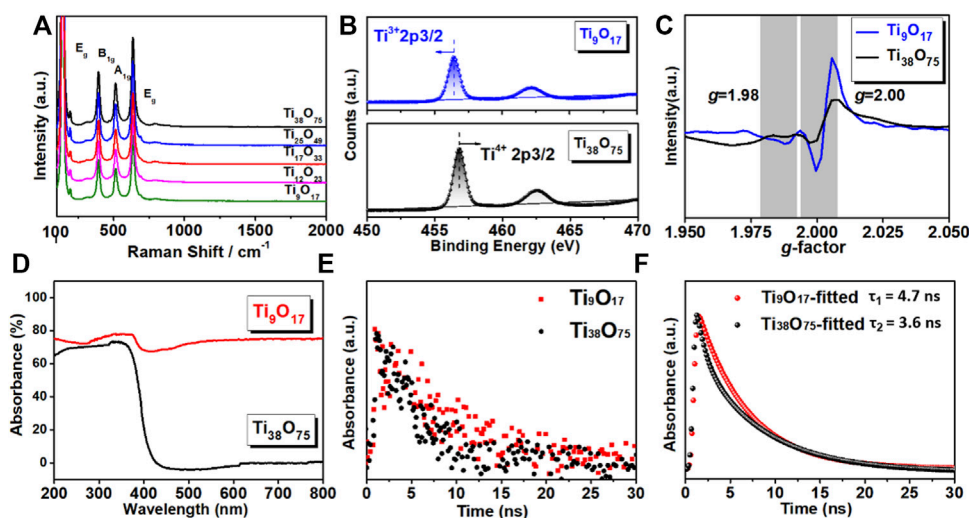


FIGURE 3

(A) Raman scattering spectra of PSC-like  $\text{Ti}_n\text{O}_{2n-1}$ . (B) XPS spectra of PSC-like  $\text{Ti}_n\text{O}_{2n-1}$  ( $n = 9$  and  $38$ ). (C) EPR spectra of  $\text{Ti}_9\text{O}_{17}$  and  $\text{Ti}_{38}\text{O}_{75}$ . (D) Ultraviolet-visible absorbance spectra. (E and F) Decay profiles and fitting curve of femtosecond transient absorption spectra.

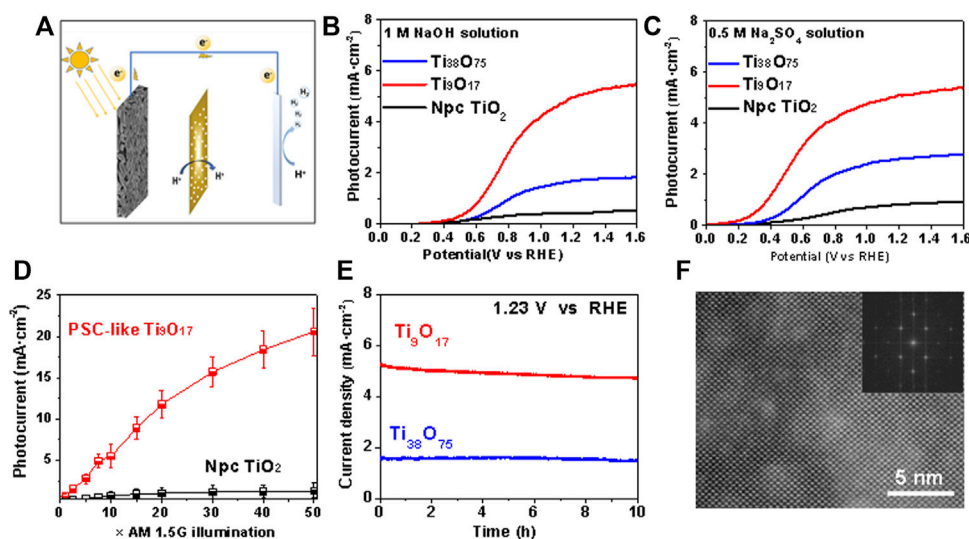


FIGURE 4

(A) The schematic diagram of photoelectrocatalysis cell. (B and C) Linear Scanning Voltammetry (LSV) curve of three electrode system using the P-SC  $\text{Ti}_n\text{O}_{2n-1}$  photoanodes for water oxidation in the 1 M NaOH and 0.5 M  $\text{Na}_2\text{SO}_4$ , respectively. ( $\text{Ti}_n\text{O}_{2n-1}$  as working electrode, Pt as counter electrode,  $\text{Hg}/\text{Hg}_2\text{Cl}_2$  as reference electrode) (D) The photocurrent with enhanced light intensity up to  $50\times\text{AM}1.5\text{G}$  sunlight using PSC-like  $\text{Ti}_9\text{O}_{17}$  and non-porous polycrystalline (Npc)  $\text{TiO}_2$  electrodes. The external bias voltage is 1.23V. (E) Photocurrent durability test of the PSC-like  $\text{Ti}_9\text{O}_{17}$  and  $\text{Ti}_{38}\text{O}_{75}$  at 1.23V. (F) The crystal structure of  $\text{Ti}_9\text{O}_{17}$  after stability test.

Figure S6, the dark current density is generally lower than  $0.5\text{ mA cm}^{-2}$ , which can be attributed to the synergy between the structural characteristics of PSC-like monolith and electronic transport. The current density is 5 times higher than that of the PSC-like  $\text{Ti}_{38}\text{O}_{75}$  electrode and  $\sim 8$  times higher than that of the Non-porous polycrystal (Npc- $\text{TiO}_2$ ) electrode. Which performance is well above that of nano-catalytic materials, demonstrating the superior activity and structural advantages of PSC-like  $\text{Ti}_9\text{O}_{17}$  crystals in photoanode.

The photocurrent of PSC-like  $\text{Ti}_9\text{O}_{17}$  increases linearly with the irradiation intensity, which photocurrent is as high as  $\sim 20\text{ mA cm}^{-2}$  under the illumination intensity of  $50\text{ AM}1.5\text{G}$  and the external bias voltage of 1.23 V. In addition, Npc- $\text{TiO}_2$  is uniformly loaded on conductive glass of  $\text{SnO}_2$  doped with fluorine (FTO) as a photoanode system, which shows a saturated photocurrent density of  $\sim 0.8\text{ mA cm}^{-2}$  under the illumination intensity of  $20\text{ AM}1.5\text{G}$  at 1.23V, indicating that its high-density grain boundary structure limits the conversion of energy. We further evaluated the durability of the

PSC-like  $\text{Ti}_9\text{O}_{17}$  photoelectrode by chronoamperometric measurement, as shown in Figure 4E, even after 10 h of operation, the photocurrent almost did not decay. It is noteworthy that the catalyst after operation still maintains uniform porous skeleton and well-defined lattice structure, as shown in Supplementary Figure S6 and Figure 4F, thus verifying the structural stability of PSC-like  $\text{TiO}_2$  as photoelectrode in the catalytic oxidation of water. In the Cs-HRTEM image of Figure 4E, the presence of residual electrolyte on the catalyst surface causes slight distortion in lattice clarity, but it would be ignored. The synergistic effect of porous microstructure, structural coherence and transport characteristics regulated by band gap engineering significantly enhanced the photocatalytic activity, resulting in an extremely high photoelectrochemical water oxidation performance.

## 4 Conclusion

In this work, we have grown PSC-like  $\text{TiO}_2$  monoliths dominated by (200) facets based on a lattice reconstruction strategy *via* solid-solid phase transformation, which has extremely high single-crystallinity and minimized grain boundary area while maintaining long-range ordered lattice structure and three-dimensional infiltration channels. It has two different lattice orientations, which is different with the porous single crystal, but still has good photoelectrochemical properties. We further introduce  $\text{Ti}^{3+}$  into the lattice by bandgap engineering to obtain a series of  $\text{Ti}_n\text{O}_{2n-1}$  monolith with the Magneli phase, and tune the electronic structure to narrow the bandgap and enhance the absorption of visible light. We evaluated the PSC-like  $\text{TiO}_2$  as a photocathode for water oxidation at 25 °C in a three electrode system and obtained a high current with no obvious attenuation after 10 h of continuous operation. We have demonstrated that the synergistic effect of long-range ordered lattice structure and porous framework can effectively enhance photocatalytic activity and structural stability, providing a new avenue for the design of novel optoelectronic materials and the tuning of surface photoreactivity.

## Data availability statement

The original contributions presented in the study are included in the article/Supplementary Material, further inquiries can be directed to the corresponding authors.

## References

- Bie, C., Wang, L., and Yu, J. (2022). Challenges for photocatalytic overall water splitting. *Chem* 8, 1567–1574. doi:10.1016/j.chempr.2022.04.013
- Bie, C., Zhu, B., Xu, F., Zhang, L., and Yu, J. (2019). *In situ* grown monolayer N-doped graphene on CdS hollow spheres with seamless contact for photocatalytic  $\text{CO}_2$  reduction. *Adv. Mater.* 31, 1902868–1902876. doi:10.1002/adma.201902868
- Chen, D., Cheng, Y., Zhou, N., Chen, P., Wang, Y., Li, K., et al. (2020). Photocatalytic degradation of organic pollutants using  $\text{TiO}_2$ -based photocatalysts: A review. *J. Clean. Prod.* 268, 121725. doi:10.1016/j.jclepro.2020.121725
- Chen, H. Y., and Ardo, S. (2018). Direct observation of sequential oxidations of a titania-bound molecular proxy catalyst generated through illumination of molecular sensitizers. *Nat. Chem.* 10, 17–23. doi:10.1038/NCHEM.2892
- Cheng, F., Lin, G., Hu, X., Xi, S., and Xie, K. (2019). Porous single-crystalline titanium dioxide at 2 cm scale delivering enhanced photoelectrochemical performance. *Nat. Commun.* 10, 3618–3619. doi:10.1038/s41467-019-11623-w
- Es-Souni, M., Kartopu, G., Habouti, S., Piorra, A., Es-Souni, M., Solterbeck, C. H., et al. (2008). Processing and thin film formation of  $\text{TiO}_2$ -Pt nanocomposites. *Phys. Status Solidi Appl. Mater. Sci.* 205, 305–310. doi:10.1002/pssa.200723181
- Faraji, M., Yousefi, M., Yousefzadeh, S., Zirak, M., Naseri, N., Jeon, T. H., et al. (2019). Two-dimensional materials in semiconductor photoelectrocatalytic systems for water splitting. *Energy Environ. Sci.* 12, 59–95. doi:10.1039/c8ee00886h
- Guo, Q., Zhou, C., Ma, Z., Ren, Z., Fan, H., and Yang, X. (2016). Elementary photocatalytic chemistry on  $\text{TiO}_2$  surfaces. *Chem. Soc. Rev.* 45, 3701–3730. doi:10.1039/c5cs00448a
- Guo, Q., Zhou, C., Ma, Z., and Yang, X. (2019). Fundamentals of  $\text{TiO}_2$  photocatalysis: Concepts, mechanisms, and challenges. *Adv. Mater.* 31, 1901997–1902026. doi:10.1002/adma.201901997
- Jacco, J. C., Loiacono, G. M., Jaso, M., Mizell, G., and Greenberg, B. (1984). Flux growth and properties of  $\text{KTiOPO}_4$ . *J. Cryst. Growth* 70, 484–488. doi:10.1016/0022-0248(84)90306-3

## Author contributions

KL wrote and revised the manuscript. FC performed the Crystal growth. YL, LL, and CW contributed to the results analysis. KX edited the manuscript. XL supervised the whole project.

## Funding

This work was supported by the National Key Research and Development Program of China (2021YFA1501500), the Natural Science Foundation of Fujian Province (2020J05082, 2020J01113), Strategic Priority Research Program of Chinese Academy of Sciences (XDB2000000), Sichuan Science and Technology Program (2019JDJQ0011, 2020ZDZX0018, and 2022YFG0001), Youth Innovation Promotion Association, Chinese Academy of Sciences (2020371, 2023393), and West Light Foundation of the Chinese Academy of Sciences.

## Conflict of interest

The authors declare that the research was conducted in the absence of any commercial or financial relationships that could be construed as a potential conflict of interest.

## Publisher's note

All claims expressed in this article are solely those of the authors and do not necessarily represent those of their affiliated organizations, or those of the publisher, the editors and the reviewers. Any product that may be evaluated in this article, or claim that may be made by its manufacturer, is not guaranteed or endorsed by the publisher.

## Supplementary material

The Supplementary Material for this article can be found online at: <https://www.frontiersin.org/articles/10.3389/fmats.2023.1177093/full#supplementary-material>

- Jiang, H. B., Cuan, Q., Wen, C. Z., Xing, J., Wu, D., Gong, X.-Q., et al. (2011). Anatase TiO<sub>2</sub> crystals with exposed high-index facets. *Angew. Chem.* 123, 3848–3852. doi:10.1002/ange.201100771
- Jin, L., Cheng, F., Li, H., and Xie, K. (2020). Porous tantalum nitride single crystal at two-centimeter scale with enhanced photoelectrochemical performance. *Angew. Chem. - Int. Ed.* 59, 8891–8895. doi:10.1002/anie.202001204
- Kou, J., Lu, C., Wang, J., Chen, Y., Xu, Z., and Varma, R. S. (2017). Selectivity enhancement in heterogeneous photocatalytic transformations. *Chem. Rev.* 117, 1445–1514. doi:10.1021/acs.chemrev.6b00396
- Li, B., Zhao, J., Onda, K., Jordan, K. D., Yang, J., and Petek, H. (2006). Ultrafast interfacial proton-coupled electron transfer. *Science* 311, 1436–1440. doi:10.1126/science.1122190
- Li, W. T., and Xie, K. (2023). Porous single crystals at the macroscale: From growth to application. *Acc. Chem. Res.* 56, 374–384. doi:10.1021/acs.accounts.2c00777
- Li, Z., Wang, S., Wu, J., and Zhou, W. (2022). Recent progress in defective TiO<sub>2</sub> photocatalysts for energy and environmental applications. *Renew. Sustain. Energy Rev.* 156, 111980. doi:10.1016/j.rser.2021.111980
- Liu, N., Xu, M., Yang, Y., Zhang, S., Zhang, J., Wang, W., et al. (2019). Au<sup>δ-</sup>-Ov-Ti<sup>3+</sup> interfacial site: Catalytic active center toward low-temperature water gas shift reaction. *ACS Catal.* 9, 2707–2717. doi:10.1021/acscatal.8b04913
- Meng, A., Zhang, L., Cheng, B., and Yu, J. (2019). Dual cocatalysts in TiO<sub>2</sub> photocatalysis. *Adv. Mater.* 31, 1807660–1807731. doi:10.1002/adma.201807660
- Qian, R., Zong, H., Schneider, J., Zhou, G., Zhao, T., Li, Y., et al. (2019). Charge carrier trapping, recombination and transfer during TiO<sub>2</sub> photocatalysis: An overview. *Catal. Today* 335, 78–90. doi:10.1016/j.cattod.2018.10.053
- Ros, C., Andreu, T., and Morante, J. R. (2020). Photoelectrochemical water splitting: A road from stable metal oxides to protected thin film solar cells. *J. Mater. Chem. A* 8, 10625–10669. doi:10.1039/d0ta02755c
- Schrauben, J. N., Hayoun, R., Valdez, C. N., Braten, M., Fridley, L., and Mayer, J. M. (2012). Titanium and zinc oxide nanoparticles are proton-coupled electron transfer agents. *Science* 336, 1298–1301. doi:10.1126/science.1220234
- Shin, H. J., Sohn, S. D., Kim, Y., Jung, S., Kang, J. S., Han, H., et al. (2022). C60 adsorbed on TiO<sub>2</sub> drives dark generation of hydroxyl radicals. *ACS Catal.* 12, 5990–5996. doi:10.1021/acscatal.2c00755
- Sorokina, N. I., and Voronkova, V. I. (2007). Structure and properties of crystals in the potassium titanyl phosphate family: A review. *Crystallogr. Rep.* 52, 80–93. doi:10.1134/S1063774507010099
- Xiao, Y., and Xie, K. (2022). Active exsolved metal–oxide interfaces in porous single-crystalline ceria monoliths for efficient and durable CH<sub>4</sub>/CO<sub>2</sub> reforming. *Angew. Chem. - Int. Ed.* 61, e202113079. doi:10.1002/anie.202113079
- Xu, F., Meng, K., Cheng, B., Wang, S., Xu, J., and Yu, J. (2020). Unique S-scheme heterojunctions in self-assembled TiO<sub>2</sub>/CsPbBr<sub>3</sub> hybrids for CO<sub>2</sub> photoreduction. *Nat. Commun.* 11, 4613–4619. doi:10.1038/s41467-020-18350-7
- Yu, X., Kim, B., and Kim, Y. K. (2013). Highly enhanced photoactivity of anatase TiO<sub>2</sub> nanocrystals by controlled hydrogenation-induced surface defects. *ACS Catal.* 3, 2479–2486. doi:10.1021/cs4005776
- Zhang, Y. C., Afzal, N., Pan, L., Zhang, X., and Zou, J. J. (2019). Structure-activity relationship of defective metal-based photocatalysts for water splitting: Experimental and theoretical perspectives. *Adv. Sci.* 6, 1900053. doi:10.1002/advs.201900053
- Zhao, Y., Zhao, Y., Shi, R., Wang, B., Waterhouse, G. I. N., Wu, L. Z., et al. (2019). Tuning oxygen vacancies in ultrathin TiO<sub>2</sub> nanosheets to boost photocatalytic nitrogen fixation up to 700 nm. *Adv. Mater.* 31, 1806482–1806489. doi:10.1002/adma.201806482